Constitutive Models of Prestressed Steel-Fiber Concrete

Christopher Caruso[1], Norman Hoffman[2], Thomas T.C. Hsu[3], and Y.L. Mo[4]

Abstract

This paper investigates the behavior of prestressed steel-fiber concrete structural elements subjected to shear action. Steel-fiber reinforcement has the potential to reduce or in some cases eliminate the need for traditional shear reinforcement (stirrups) in some structures. Minimizing the need for traditional shear reinforcement would thus result in a reduction in time and labor costs associated with placement and fabrication. Prestressed concrete structures such as deep shear walls, box bridges, nuclear containment vessels and off-shore structures can be idealized as assemblies of shear elements. Full understanding of the shear behavior of elements is necessary to accurately predict behavior of these prestressed structures using the Softened Membrane Model (SMM). The initial results from a series of tests are presented and are used to extend the (SMM) to prestressed steel-fiber concrete by developing new constitutive laws, including the stress-strain relationship of embedded prestressing strand and the softening coefficient.

Introduction

Prestressed concrete is one of the most common building materials found in highway infrastructure today. It takes advantage of the superior tensile strength of prestressing strands to improve the weak tensile strength of regular reinforced concrete and is commonly found in structural elements under combined tensile and compressive stresses such as highway bridge girders. In order to accurately model the behavior of prestressed concrete under flexure and shear, understanding of its constitutive models is essential. This paper is part of a larger research project devoted to modeling and explaining the behavior of prestressed steel-fiber concrete under shear, but only focuses on behavior under sequential tension and compression.

Extensive study of the constitutive models of plain reinforced concrete was necessary before any significant studies of prestressed concrete could be conducted. Robinson and Demorieux (1968) discovered that the compressive strength of a concrete element was diminished if it was under tensile stress in the perpendicular direction. They observed this "softening" effect in several I-beam tests but were unable to quantify it.

Vecchio and Collins (1981) developed the Compression Field Theory (CFT) while studying the softening of pure concrete. This model was capable of predicting the post-cracking behavior of

[1] *Department of Engineering, Swarthmore College, Swarthmore, PA, 19081, USA*
Email: ccaruso1@swarthmore.edu, Ph# 631-276-9342
[2] *Department of Civil and Environmental Engineering, University of Houston, Houston, TX 77204-4403, USA*
Email: eshoffman007@aol.com, Ph# 409-737-9322
[3] *Department of Civil and Environmental Engineering, University of Houston, Houston, TX 77204-4403, USA*
Email: tshu@uh.edu , Ph# 713-743-4268, Fax# 713-743-4260
[4] *Department of Civil and Environmental Engineering, University of Houston, Houston, TX 77204-4403, USA*
Email: ymo@uh.edu , Ph# 713-743-4274, Fax # 713-743-4260

reinforced concrete elements under shear up to ultimate strength. Vecchio and Collins (1986) later developed the Modified Compression Field Theory (MCFT) to account for evidence that cracked concrete had a non-zero tensile strength, contrary to their assumptions in CFT.

Another model named the "Rotating-Angle Softened Truss Model" (RA-STM) was developed at the University of Houston (Pang, 1991; Belarbi and Hsu, 1994 and 1995) to model reinforced concrete under shear. The RA-STM assumed that cracks in reinforced concrete form in the direction of principle compressive stress after cracking. This, however, makes it impossible to account for the concrete's contribution to shear resistance after cracking. Pang (1991) developed the "Fixed-Angle Softened Truss Model" (FA-STM) to account for this concrete contribution by assuming that the direction of cracks can be different from that of principle compressive stress in the cracked concrete.

A study of the post-peak behavior of reinforced concrete by Hsu and Zhu (2002) resulted in development of the "Softened Membrane Model" (SMM). This model incorporated Poisson effects of cracked reinforced concrete into a unified analytical solution for predicting the behavior of reinforced concrete panels under shear to ultimate failure.

A research team at the University of Houston (Laskar et al., 2006) developed the Softened Membrane Model for Prestressed Concrete (SSM-PC) as an extension to the SMM (Hsu and Zhu, 2002). They also performed experiments on 2D prestressed concrete panel elements in the Universal Panel Tester at the University of Houston to obtain the constitutive models of prestressed concrete under sequential loading. These tests showed that prestress increases concrete compressive strength under sequential loading by 15%.

Another recent development in concrete technology is the inclusion of steel fibers in concrete mix to reduce crack propagation. Concrete of this type is typically referred to as steel-fiber concrete (SFC). The load-bearing capacity and behavior of SFC has been studied extensively, but study of steel-fiber reinforcement in prestressed concrete has been limited.

Romualdi and Mandel (1964) considered the use of randomly-oriented short steel fibers as a substitute for long wires oriented parallel to the direction of principal stress in concrete as a method of fracture arrest. Their study of beam and indirect tension (splitting) mechanisms confirmed ideas that steel-fiber reinforcement could provide some load-bearing capacity to concrete after cracking.

Abrishami and Mitchell (1997) found that steel fibers significantly reduced the propagation of cracks in normal and high-strength concrete elements under pure tension. They also found that tension elements containing steel-fiber reinforcement carried additional load after yielding of the main reinforcing bars where regular reinforced concrete elements did not.

Kützing and König (1999) proposed that the presence of steel fibers in concrete contributed most effectively to post-yield behavior and had little effect on the maximum strength of concrete. For this reason, they proposed that the analysis of steel-fiber concrete be based on fracture mechanics parameters such as fracture energy and characteristic length instead of the strength characteristics of concrete. They developed an appropriate analytical model relating major crack width in steel-fiber concrete to the stress it carried.

A research team at the University of Houston (Dhonde, H. et al., 2005) investigated the practicality and strength of steel-fiber reinforcement in the Texas Traditional Concrete (TTC) mix used by the Texas Department of Transportation (TxDOT) on major highway projects. They found that the inclusion of steel fibers in TTC resulted in a 25% increase in tensile strength on average in addition to notable improvements in flexural strength and member ductility. They also studied the shear strength of SFC in prestressed highway I-beams by constructing and testing prototype beams to failure. They found that beams containing steel-fiber reinforcement had comparable shear strengths to those without and that the highest strength steel-fiber beam tested had no transverse reinforcement at all, proving that SFC has the potential to replace traditional shear stirrups in prestressed highway I-beams

Objective

This paper studies the behavior of prestressed steel-fiber concrete (PSFC) by establishing the constitutive models for prestressing tendons and steel-fiber concrete. These models are determined experimentally using full-scale testing of 2D membrane elements (panels) of prestressed steel-fiber concrete. The effective structural performance improvements afforded by steel-fiber reinforcement to prestressed concrete membrane elements will then be evaluated through a comparison to previous studies of prestressed concrete panels conducted under the same testing procedure.

Constitutive Models of Prestressed Concrete

Applied Tensile Stress-Strain Relationships

A research team at the University of Houston (Laskar et al., 2006) obtained the experimental tensile stress-strain relationships of several prestressed concrete panels, as shown in Fig. 2.1, each containing a different ratio of prestressing steel to concrete. The panels TE-6, TE-3, and TE-7 each had a reinforcing ratio of 0.30%, 0.59%, and 1.18%, respectively. Fig 2.1 shows that the corresponding tensile stresses at a tensile strain of 0.02 were 5.5, 11.0, and 21.5 MPa, respectively. These stresses are roughly proportional to the prestressing steel ratios in each panel. They derived sets of constitutive models for concrete and prestressing tendons from these experimental stress-strain relationships using equilibrium and strain compatibility as shown in the following sections.

Smeared (Average) Stress-Strain Relationships of Concrete in Tension

The analytical model for the tensile stress-strain relationship of prestressed concrete contains three stages. First, the concrete starts at its initial state of prestress under compressive stress due to the prestressing tendon forces. The first stage of tensile loading is decompression, where the concrete unloads its compressive stress until its normal stress is zero. Following the decompression stage, stage two is characterized by further tensile strain which causes linearly-increasing tensile stress in the concrete until cracking occurs. In the third stage, the concrete has passed its cracking strain and tensile stress in the concrete then decreases exponentially under increasing tensile strain. Fig 2.2 illustrates these three stages of the tensile stress-strain relationship of concrete, labeled UC, T1, and T2 respectively. The model for these three stages is presented in the following three equations:

$$\text{Stage UC:} \quad \sigma_c = E'_c(\bar{\varepsilon}_c - \bar{\varepsilon}_{ci}) + \sigma_{ci}, \qquad \bar{\varepsilon}_c \le \bar{\varepsilon}_{cx} \tag{1}$$

$$\text{Stage T1:} \quad \sigma_c = E''_c(\bar{\varepsilon}_c - \bar{\varepsilon}_{cx}), \qquad \bar{\varepsilon}_{cx} < \bar{\varepsilon}_c \le \varepsilon_{cr}, \tag{2}$$

$$\text{Stage T2:} \quad \sigma_c = f_{cr}\left(\frac{\varepsilon_{cr}}{\bar{\varepsilon}_c}\right)^{0.5}, \qquad \bar{\varepsilon}_c > \varepsilon_{cr}. \tag{3}$$

Average Stress-Strain Relationships of Prestressing Tendons Embedded in Concrete

The constitutive models for prestressing tendons embedded in concrete describe two stages of behavior: First, stress and strain are linearly related in the tendons by the elastic modulus of steel. Second, the stress-strain relationship becomes nonlinear because the steel has exceeded yield stress. The following equations describe these two stages of prestressing tendon behavior.

$$f_{ps} = E_{ps}\bar{\varepsilon}_s, \qquad \bar{\varepsilon}_s < \frac{0.7 f_{pu}}{E_{ps}}, \tag{5}$$

$$f_{ps} = \frac{E''_{ps}\bar{\varepsilon}_s}{\left[1 + \left(\frac{E''_{ps}\bar{\varepsilon}_s}{f'_{pu}}\right)^5\right]^{\frac{1}{5}}}, \qquad \bar{\varepsilon}_s \ge \frac{0.7 f_{pu}}{E_{ps}}. \tag{6}$$

Experimental Program

To establish the constitutive models, a prestressed steel-fiber concrete panel (TEF-1) containing 0.5% steel fibers by weight was tested. The layout and dimensions of this panel are shown in Fig 3.1. The compression reinforcement bars were ten #4 mild steel bars arranged parallel to the *t* direction in two layers. Both panels also contained ten prestressing tendons arranged parallel to the *l* direction in two layers. During testing, tensile loads were applied parallel to the *l* direction on the right and left sides of the panel, while compressive loads were subsequently applied parallel to the *t* direction on the upper and lower sides.

Concrete

The concrete mix design was proportioned for a target compressive strength of 41.4 MPa (6 ksi) and a slump of 178 mm (7 in). The mix proportions by weight were 1:2.64:2.93 for cement, fine aggregate (sand), and coarse aggregate, respectively. Type I Portland Cement was used and the water-cement ratio for the mix was 0.6.

Prestressing Tendons

Steel prestressing tendons with a diameter of 0.6 in. were arranged parallel to the *l* direction. The tendons were prestressed to an average tensile load of 141 kN (31.7 kips) and anchored to U-Shaped steel brackets embedded in opposite sides of the panel.

Fabrication

The form for the concrete panels was constructed with steel plate and bolted together. Both ends of the compression reinforcement bars were welded to steel plate-brackets that bolted into the form. A special steel jig was used to facilitate proper alignment and welding of the compression bars to these plate-brackets.

The steel U-shaped brackets used to anchor the prestressing tendons were welded together from three separate pieces and then bolted into the form. Lengths of metal wire-conduit were cut to length and fit into the U-shaped brackets to run horizontally across the form and encase the prestressing tendons that would be added after pouring. A circular metal bar was placed inside each conduit tube so that they retained proper form during pouring. A hole was also drilled in each end of each conduit to accept a lexan grout tube, which would later be used to deliver a self-compacting grout into the conduit.

Test Setup

Testing of the panel was performed using the Universal Element Tester (UET) at the University of Houston. The UET is designed to accept concrete panels 1398 mm(55 in.) square and up to 406 mm (16 in.) thick and load them in any combination of shear, tension and compression (uniaxial or biaxial), bending, and torsion. The UET consists of a 4.8m. x 4.8 m (15.7 ft x 15.7 ft) steel frame that houses 37 in-plane jacks of 890 kN (100-ton) capacity each and 3 in-plane rigid links. The panel was fitted with 5 steel yokes bolted on each side, allowing it to be attached at 40 points to the jacks and rigid links in the UET.

The sequential loading test was controlled by custom computer software and electronic servo jack controls. The UET was to operate in both a load-controlled mode and a strain-controlled mode. The panel was first to be loaded on the right and left sides in tension to 178 kN (40 kips) in load control mode, then strained to 2% in strain control mode. Once 2% tensile strain had been reached, a compressive load of 133 kN (30 kips) would be applied to the top and bottom edges in load control mode while keeping tensile strain constant. Upon reaching 133 kN of compressive load, the tester would switch to strain-controlled mode in compression and apply more compressive load until ultimate failure had been reached.

The data collected in the panel test included horizontal, vertical, and diagonal smeared panel strains, crack widths, and jack loads sampled every ten seconds. Ten linearly variable differential transformers (LVDT's) were mounted symmetrically on each of both sides of the panel, as shown in Fig. 3.2, using aluminum brackets and all-thread rod. Eight LVDT's measured horizontal strain, eight LVDT's measured vertical strain, and the remaining four measured diagonal strain. The use of multiple LVDT's along both principal axes and the diagonals allowed an average strain to be obtained, which provided more accurate strain data. Fig. 3.2 also shows that the instrumentation is mounted in the center of the panel so as to enclose a test-section 800 mm (31.5 inches) square. This placement ensures the LVDT measurements are far enough from the edges of the panel so that they are free from disturbance due to unpredictable boundary effects.

Experimental Results

The test program for TEF1 was not completed as planned due to premature failure of the prestressing tendons. The first tendon failure occurred at an experimental tensile strain of 0.00088, followed by additional tendon failures at strains of 0.005216, 0.01298, and an ultimate failure strain of 0.01427. It was also noted shortly before the first tendon failure that severe cracking had begun around the boundary of the panel as shown in Fig. 4.1.

A plot of the principal tensile stress vs. strain for panel TEF1 is shown in Fig. 4.2 against a PC panel (TE5) tested at the University of Houston (Laskar et al., 2006) with similar prestress level, reinforcing ratio, and cylinder break strength. Both panels had the same number of prestressing tendons, all of which were prestressed to roughly the same tensile load (140 ± 2 kN). Both panels had the same dimensions (1397 mm. x 1397 mm. x 178 mm) and roughly the same compressive strength ($f_c^{'} = 35.2 \pm .5$ MPa) and corresponding strain ($\varepsilon_o = 0.00218 \pm 10^{-5}$). The three tendon failures are clearly noticeable in Fig. 4.2 as sharp drops in stress followed by gradual reloading. Also notice that for each measured strain above cracking, TEF1 has a higher applied stress than TE5. This was also expected because severe cracks formed outside the test section and thus their contribution to the panel's total tensile strain was not recorded. The result was that an undesirably small amount of the tensile strain was measured. Strain applied after cracking had the effect of opening the boundary cracks further and giving less strain in the measured region.

Another factor that contributed to premature tendon failure was inadequate grouting of the conduit tubes enclosing the prestressing tendons. After the tendons were prestressed prior to testing, self-compacting grout was poured into the space enclosing the tendons to improve transfer of the applied load to the concrete. However, short (~13 mm) lengths of tendon between the edge of the panel and the prestressing chucks did not receive grout. These short lengths of tendon were therefore under much higher strain than predicted because they were not bonded to the panel concrete, making them prone to failure at lower applied loads. It was indeed found to be the case that tendon failure occurred in these ungrouted regions of the prestressing tendons.

The final experimental complication encountered during testing was that the LVDT's were not oriented perfectly parallel to the surface of the panel. Due to small abnormalities on the panel surface, the right-angle brackets that held the LVDT's did not always sit flush against the panel. This condition was problematic because the LVDT rods did not all align perfectly parallel with the actual LVDT's, making the rod prone to binding and slipping against the LVDT housing. This binding/slipping phenomenon occurred in several of the horizontal LVDT's during testing in the panel's elastic region, resulting in a series of shifted strain data points. It was noted that the slope of the shifted points matched the slope of the unshifted points. Furthermore, no data-shift was observed in the diagonal LVDT's, which also record horizontal strain to a lesser degree. Since the diagonal LVDT data was acceptable and the slope of the shifted LVDT data matched that of the surrounding elastic region points, it was determined that the shift was caused by binding in the misaligned LVDT's. Since the shift did not reflect aberrant panel behavior, it was determined that these points could be shifted over to where they would line up with surrounding unshifted data and was carried out accordingly.

A plot of the smeared (average) tensile stress vs. strain in concrete is shown in Fig. 4.3 for panel TEF1 against panel TE5 and its analytical model. The concrete stresses in TEF1 are considerably lower than in TE5 in the elastic region ($\varepsilon < 5\times10^{-4}$). As the concrete strains increase, stresses in TEF1 and TE5 converge with TE5 remaining slightly higher at the last data point. Also note that TEF1 and TE5 have close elastic moduli, however TEF1 has an unexpected shift in strain during the decompression stage.

Experimental plots of stress vs. strain for prestressing tendons embedded in concrete are shown in Fig. 4.4 for panels TEF1 and TE5 (denoted with "Exp) along with the analytical model of TE5. The tendon failures in TEF1 are also apparent in this plot through sharp discontinuities in stress. As expected, the average tendon stresses are considerably higher in TEF1 than in TE5 after cracking. However, both TE5 and TEF1 show nearly identical behavior prior to cracking ($\bar{\varepsilon}_c \approx 0.007$). Furthermore, tendon behavior in the elastic region is well-predicted by the analytical model for both panels.

A comparison of the compressive stress-strain relationships for various steel-fiber concrete cylinders and Texas traditional concrete cylinders is shown in Fig. 4.5. Cylinders TEF1-1C and TEF1-2C were created from the two concrete batches used to fabricate TEF1. Cylinders TTFRC1, TTFRC2, and TTFRC3 were Texas traditional concrete mixes containing steel fibers tested at the University of Houston (Dhonde, H. et al., 2005), as were cylinders TTC1 and TC-Ref, which were Texas traditional concrete mixes without steel fibers. Conclusions about the maximum compressive strength of steel-fiber concrete are not possible from Fig. 4.5 because of the wide spread of concrete strengths attained, however important conclusions can be drawn about post-peak behavior of steel-fiber concrete under compression. The plots show that mixes with steel fibers tend to have less curvature near their maximum strength and, on average, undergo more strain between the elastic limit and maximum strength. Additionally, steel-fiber mixes reached ultimate failure at higher strains on average than the non-fiber mixes.

Discussions

The test data for panel TEF1 accurately reflects the panel's behavior as observed during testing. Since the addition of steel fibers is the only real difference between TEF 1 andTE5, the premature tendon failure in TEF1 must be attributed to the steel fibers. Since TEF1 was the first prestressed steel-fiber panel ever tested at the University of Houston, its behavior could not be accurately predicted beforehand and hence the panel was not designed differently to account for the added strength due to steel fibers. In this case, the boundaries of the panel need to be stronger.

No quantitative conclusions concerning the strength of PSFC panel can be made based on the results of TEF1, however many lessons applicable to PSFC panel design and testing were learned from the experiment. Cracking was concentrated at the boundaries of the panel and the severe cracks ran through several holes drilled near the panel edge. These holes were used to accept bolts that would apply a compressive stress to the panel where the tensile jack loads were applied, thereby increasing the transfer of tensile load from the jacks to the concrete in the panel. These bolts were not sufficiently torqued and consequently the load transfer from jacks to concrete was inadequate. This caused a disproportionately high load to transfer into the prestressing tendons and thus caused them to fail prematurely.

A proposed change to the panel design for future PSFC panels includes applying the maximum allowable torque to the compressive load bolts described previously so as to increase the load transfer to the concrete through friction. To further increase this frictional load transfer, the space between the compression plates and the concrete panel should be filled with grout so a better bond is made between the point of force transfer (jack to panel) and the panel itself.

A possible explanation for the formation of severe cracks at the panel boundary was the significant concrete blow-out that occurred when the holes described previously were drilled to accept bolts used for frictional load-transfer. A hammer drill was used to drill these holes after the concrete had hardened. The holes were also drilled continuously from one side of the panel to the other so as to avoid the risk of drilling two misaligned holes to meet from both sides. The problem encountered in this method was that pieces of concrete broke off the back surface of the panel as the drill emerged out the opposite side. The result was that the panel was weakened in those regions. Since severe cracks propagated through the line of these holes, it was determined that the holes were indeed weak regions, as expected, and needed to be strengthened in order to lessen their vulnerability to cracking.

An alternative to drilling these holes in the cured concrete is to fabricate plastic tubes to wire into the form prior to pouring so that the concrete is cast around the holes and drilling becomes unnecessary. The tubes must be flexible material so they do not provide significant resistance to the clamping force that will be applied to them when the compression plates are fastened in place. This method will eliminate the blow-out that weakened the hole-regions in TEF1 and decrease the likelihood of cracking through these regions.

Conclusions

Prestressed steel-fiber concrete panels tested in sequential loading (tension and compression) experienced premature tendon failure during the tensile-loading stage due to insufficient boundary strength. Improvements to the panel design are therefore necessary to ensure the success of future prestressed steel-fiber concrete panel tests.

Suggested Improvements

1. Application of maximum allowable compression to plate-bolt assemblies intended to transfer tensile loads from the Universal Element Tester jacks to the test-panel's concrete.
2. Application of a high-strength grout mix to the bonding surface between the panel and these plate-bolt assemblies as a measure to further improve tensile load transfer to the panel concrete.
3. Use the following improved method for creating holes in the panel necessary for these plate-bolt assemblies: Fabricate lexan tubes to-size and wire them into the form prior to pouring the panel, allowing the holes to be pre-formed during pouring and minimize the concrete blow-out associated with drilling these holes after the panel has been poured.

Acknowledgements

The research study described herein was sponsored by the National Science Foundation under the Award No. EEC-0649163. The opinions expressed in this study are those of the authors and do not necessarily reflect the views of the sponsor.

Notation

E_c'	=	Decompression modulus of concrete taken as $\dfrac{2f_c'}{\varepsilon_0}$
E_c''	=	Modulus of concrete taken as $\dfrac{f_{cr}}{\varepsilon_{cr} - \bar{\varepsilon}_{cx}}$
E_{ps}	=	Modulus of prestressing tendons taken as $200\ \text{GPa}\ (29000\ \text{ksi})$
E_{ps}''	=	Modulus of prestressing tendons taken as $209.2\ \text{GPa}\ (30345\ \text{ksi})$
$f_c^{'}$	=	The compressive strength of the concrete
f_{cr}	=	Concrete cracking stress taken as $0.31\sqrt{f_c'}$ (f_c' and $\sqrt{f_c'}$ are in MPa)
f_{pu}	=	Ultimate strength of prestressing tendons taken as $1862\ \text{MPa}\ (270\ \text{ksi})$
f_{pu}'	=	Revised strength of prestressing tendons taken as $1793\ \text{MPa}\ (260\ \text{ksi})$
$\bar{\varepsilon}_c$	=	Normal strain in concrete
$\bar{\varepsilon}_{ci}$	=	Initial normal strain in concrete due to prestress
ε_{cr}	=	Concrete cracking strain taken as 0.00008
$\bar{\varepsilon}_{cx}$	=	Extra strain calculated by $\bar{\varepsilon}_{ci} - \dfrac{\sigma_{ci}}{E_c'}$
ε_o	=	Compressive concrete strain at which maximum compressive cylinder strength ($f_c^{'}$) is attained
σ_c	=	Normal stress in concrete
σ_{ci}	=	Initial normal stress in concrete

Appendix I. References

Abrishami, H.H., and Mitchell, D. (1997), “Influence of Steel Fibers on Tension Stiffening,” *ACI Structural Journal*, Vol. 94, No.6, November-December 1997, pp. 769-776.

Belarbi, A. and Hsu, T. T. C. (1994), “Costitutive Laws of Concrete in Tension and Reinforcing Bars Stiffened by Concrete,” *Structural Journal of the American Concrete Institute*, Vol. 91, No. 4, pp. 465-474.

Belarbi, A. and Hsu, T. T. C. (1995), "Constitutive Laws of Softened Concrete in Biaxial Tension-Compression," *Structural Journal of the American Concrete Institute*, Vol. 92, No. 5, pp. 562-573.

Dhonde, H., Mo, Y.L., and Hsu, Thomas T.C. (2005), "Fiber Reinforcement in Prestressed Concrete Beams," Technical Report (No. FHWA/TX-06/0-4819-1) presented to Texas Department of Transportation (TxDOT), Research and Technology Implementation Office, Austin, TX.

Hsu, T. T. C. (1993), *Unified Theory of Reinforced Concrete*, CRC Press, Inc., Boca Raton, FL, 336 pp.

Kützing, L., and König, G. (1999), "Design Principals for Steel Fibre Reinforced Concrete – A Fracture Mechanics Approach," *Leipzig Annual Civil Engineering Report LACER*, Vol. 4, 1999, pp. 175-184.

Laskar, A., Wang, J., Hsu, T.C.C, and Mo, Y.L. (2006), "Rational Shear Provisions for AASHTO LRFD Specifications," Technical Report (No. FHWA/TX-07/0-4759-1) presented to Texas Department of Transportation (TxDOT), Research and Technology Implementation Office, Austin, TX.

Pang, X. B. (1991), "Constitutive Laws of Reinforced Concrete in Shear," *Ph.D. Dissertation*, Department of Civil and Environmental Engineering, University of Houston, Houston, TX.

Robinson, J. R. and Demorieux, J. M. (1968), "Essai de Traction-Compression sur Modeles d'Ames de Poutre en Beton Arme," Compte Rendu Partiel I, U.T.I., Institut de Recherches Appliquees du Beton Arme, Paris, France, 43 pp.

Romualdi, J.P., and Mandel, J.A. (1964), "Tensile Strength of Concrete Affected by Uniformly Distributed and Closely Spaced Short Lengths of Wire Reinforcement," ACI Journal, *Proceedings* Vol. 61, No. 6, June 1964, pp. 657-670.

Vecchio, F. J. and Collins, M. P. (1981), "Stress-Strain Characteristic of Reinforced Concrete in Pure Shear," IABSE Colloquium, Advanced Mechanics of Reinforced Concrete, Delft, *Final Report*, International Association of Bridge and Structural Engineering, Zurich, Switzerland, pp. 221-225.

Vecchio, F. J. and Collins, M. P. (1986), "The Modified Compression Field Theory for Reinforced Concrete Elements Subjected to Shear," *ACI Journal*, Vol. 83, No. 2, pp. 219-231.

Zhu, R. R. H., and Hsu, T. T. C. (2002), "Poisson Effect of Reinforced Concrete Membrane Elements," *Structural Journal of the American Concrete Institute*, Vol. 99, No. 5, pp. 631-640.

Appendix II. Figures

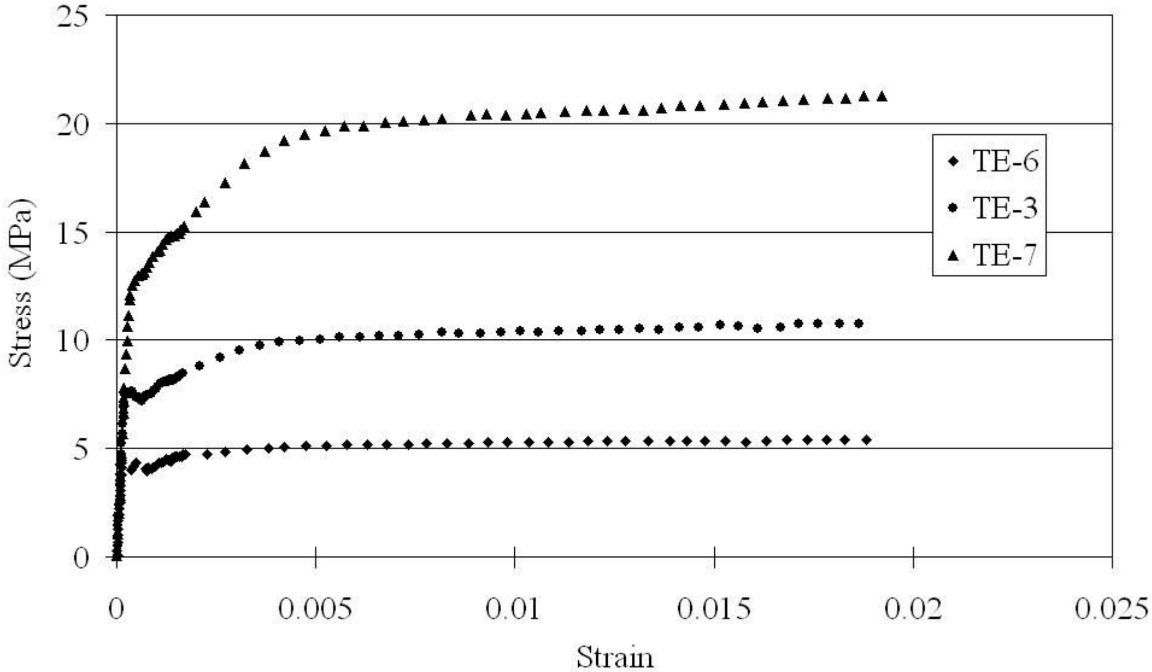

Fig 2.1 - Experimental tensile stress-strain relationship of prestressed concrete panels TE-6, TE-3, and TE-7 tested at the University of Houston (Laskar et al., 2006).

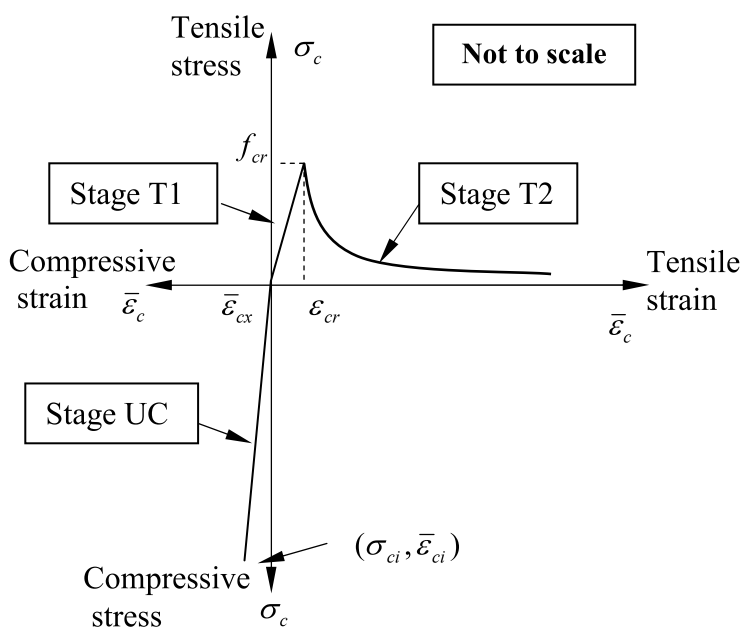

Fig 2.2 - Smeared stress-strain relationships of concrete in tension.

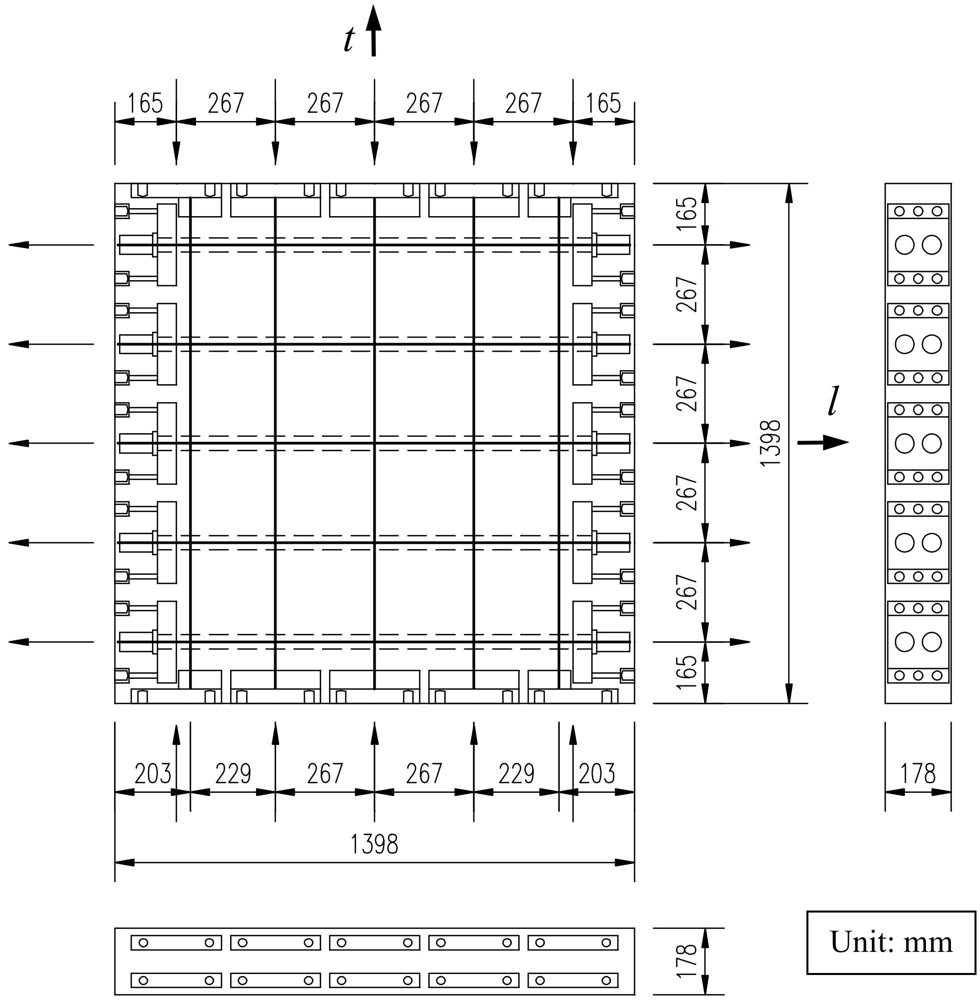

Fig. 3.1 - Steel reinforcement layout and dimensions of panel TEF1.

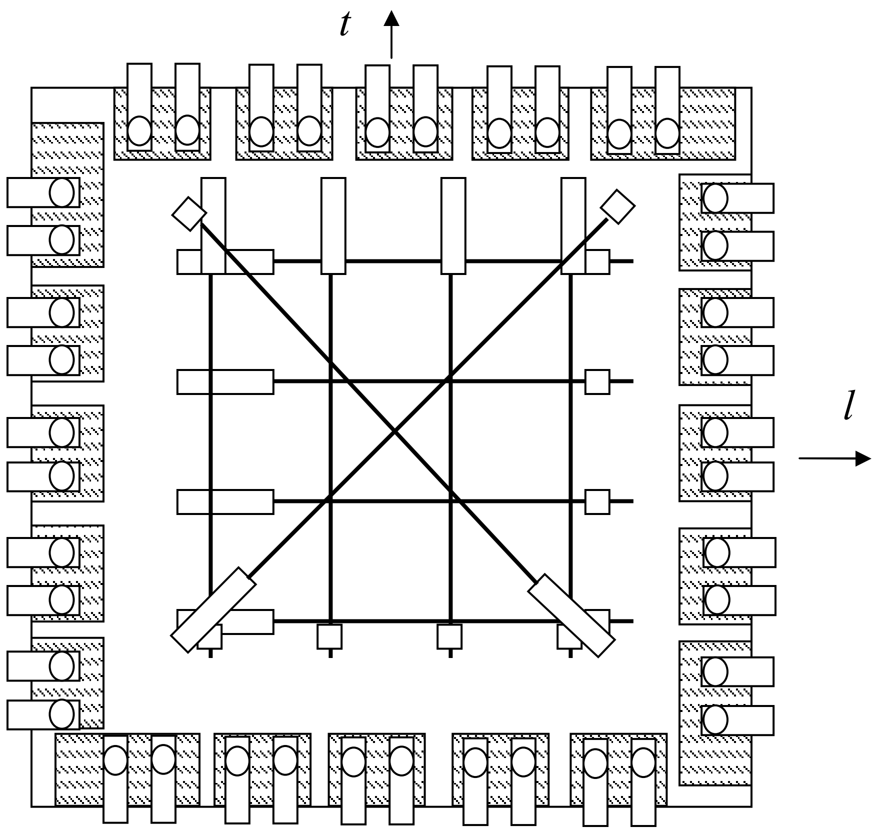

Fig. 3.2 - Test panel TEF1 mounting hardware and LVDT arrangement

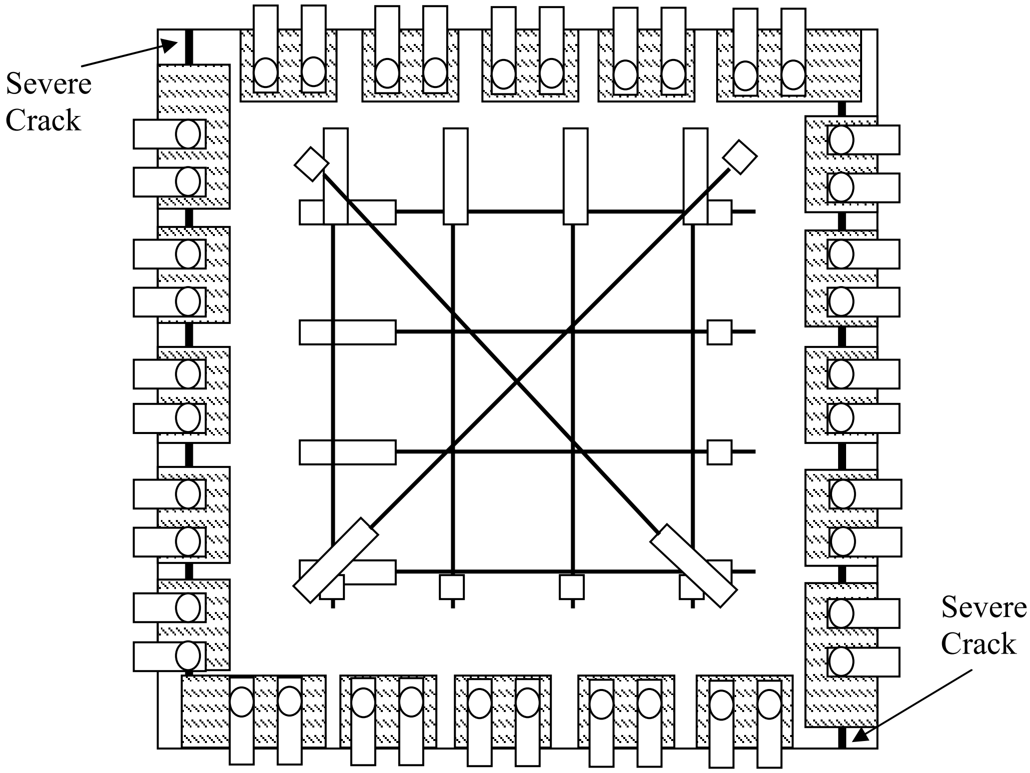

Fig. 4.1 - Diagram of panel TEF1 showing location of first major tensile cracks.

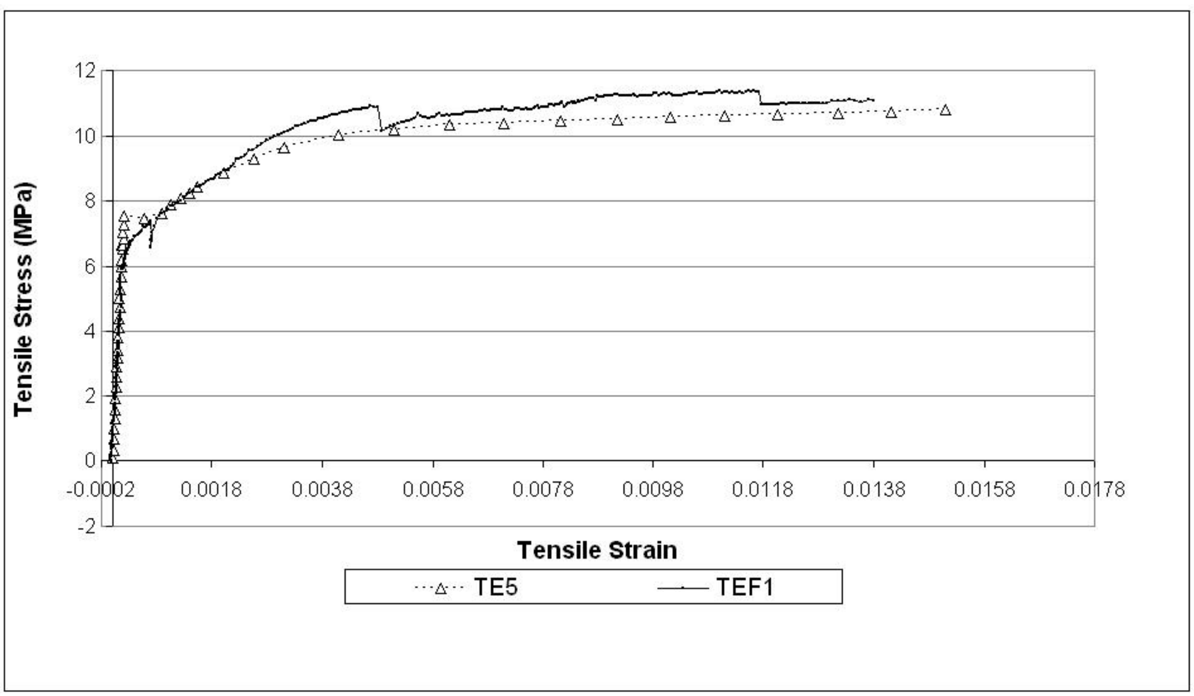

Fig. 4.2 - Principal tensile stress vs. strain for PC panel (TE5) and PSFC panel (TEF1).

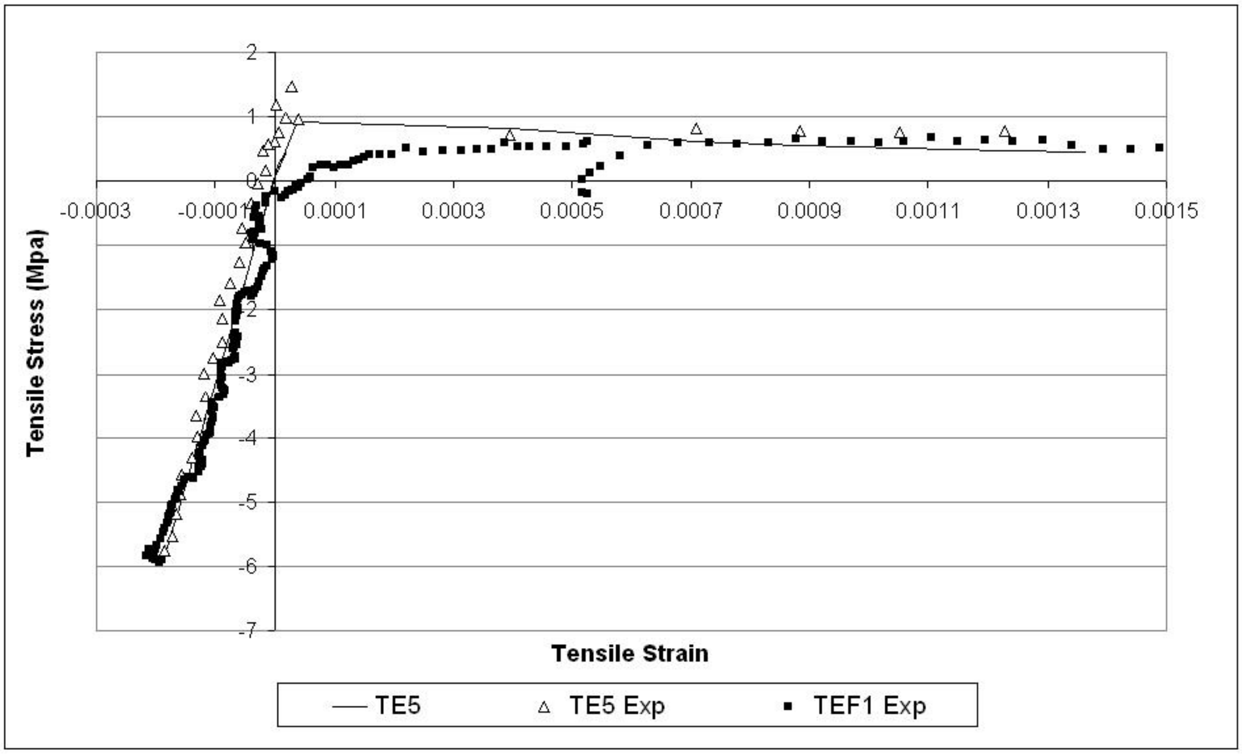

Fig. 4.3 - Tensile stress-strain curve for concrete in PSFC (TEF1 Exp) against curves for PC (TE5 Exp) and PC analytical model (TE5).

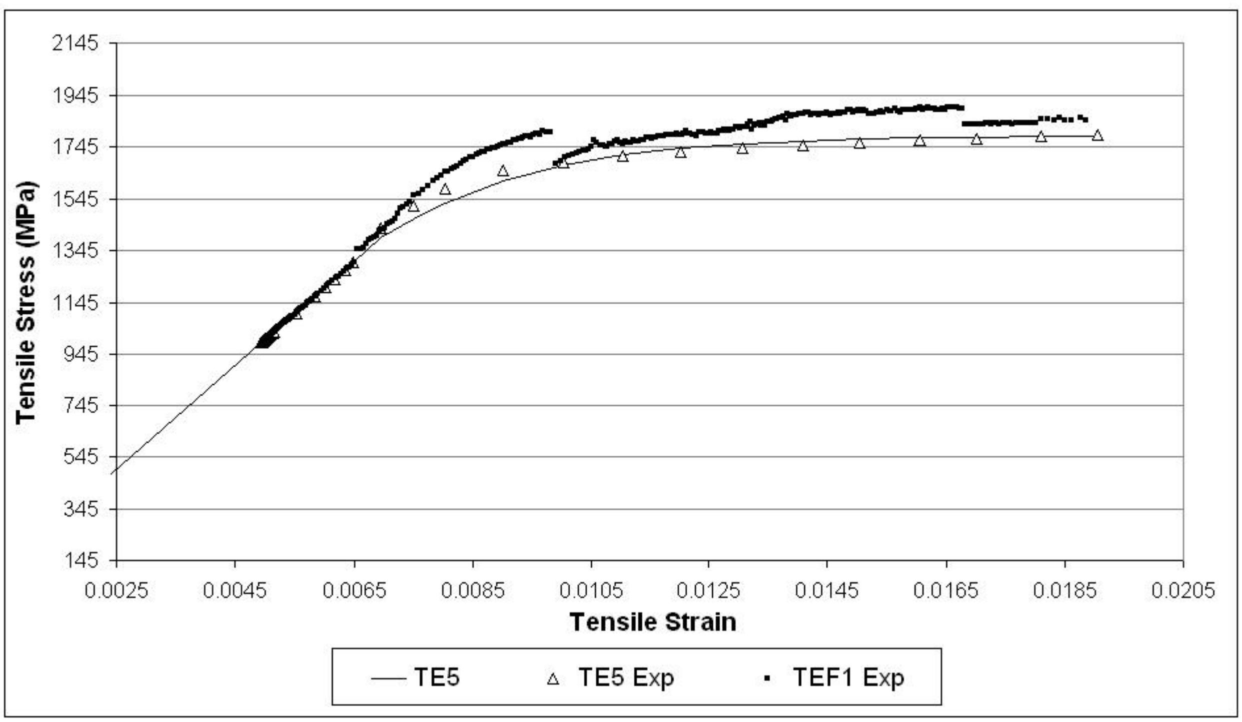

Fig. 4.4 - Average tensile stress-strain curve for prestressing tendons in PSFC (TEF1 Exp) plotted against experimental curve for TE5 (TE5 Exp) and its analytical model (TE5).

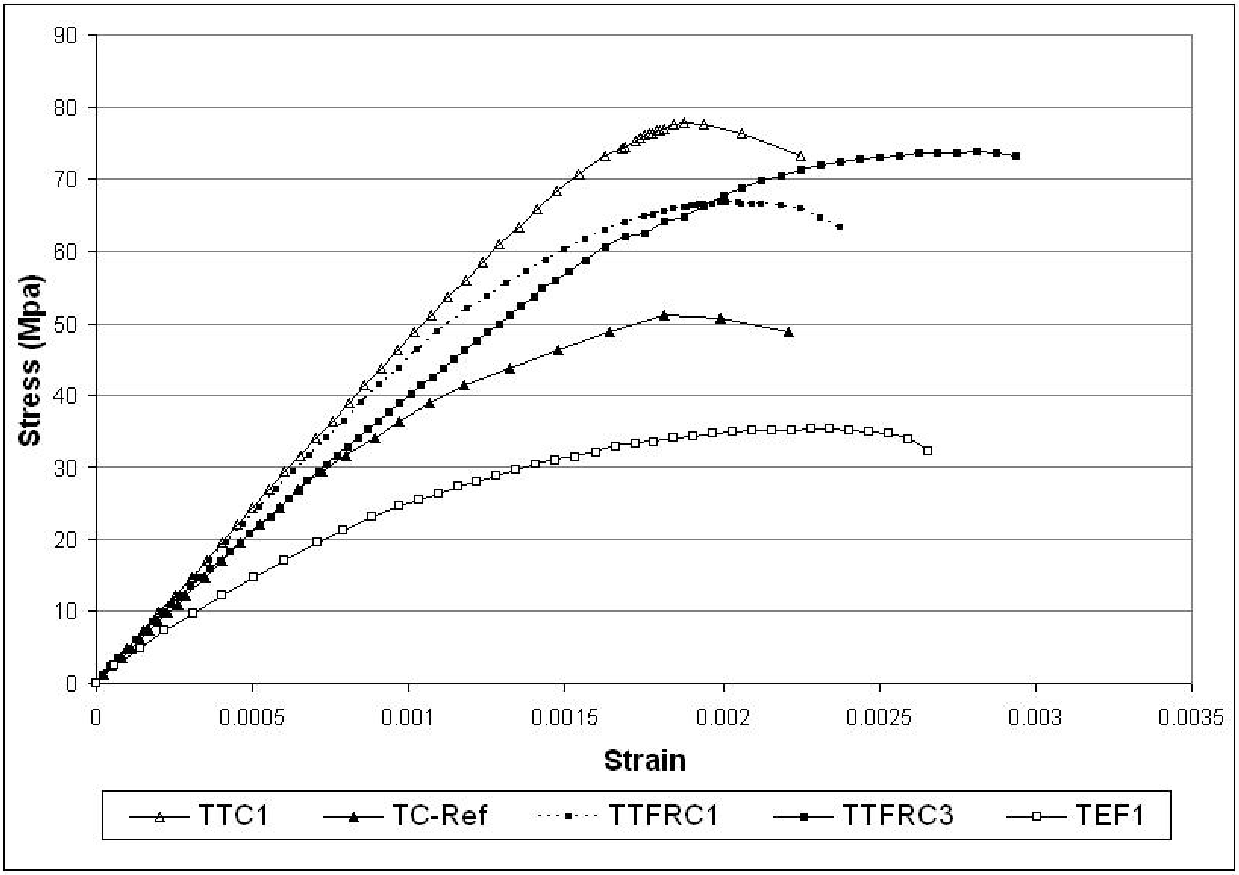

Fig. 4.5 - Compressive stress-strain curves at 28 days for Texas traditional concrete mixes (TTC1, TC-Ref), Texas traditional steel-fiber concrete mixes (TTFRC1, TTFRC3), and experimental steel-fiber concrete mix (TEF1).